# 28

# Fuel-cell Power Electronics for Distributed Generation

**S. K. Mazumder, Ph.D.**
*Department of Electrical and Computer Engineering, Director Laboratory for Energy and Switching-Electronics Systems (LESES), University of Illinois, Chicago, Illinois, USA*



## 28.1 Distributed Generation

On-site power generation (often called as distributed generation (DG) [1, 2]) using alternative/renewable-energy technologies, as illustrated in Fig. 28.1, can minimize environmental pollution and reduce our dependence on fossil fuels. Distributed energy resources (DER) are parallel and stand-alone electric generation units located within the electric distribution system near the end user. The distributed energy resources, if properly integrated can be beneficial to electricity consumers and energy utilities, providing energy independence and increased energy security. Each home and commercial unit with DER equipments can be a micro-power station, generating much of the electricity it needs on-site and sell the excess power to the national grid.

Table 28.1 provides information regarding commercially available equipment for DER [1, 2] and for those technologies still undergoing development. Some of these technologies are listed in both categories because they are commercially available and undergoing further research and development as well. There are several customer DG applications including (i) allowing customers to continuously generate their own electricity, with or without grid backup; (ii) permitting customers to generate power while serving their thermal and/or cooling loads; (iii) generating a portion of electricity on-site to reduce the amount of electricity purchased during peak-price periods; (iv) licensing customers to sell excess generation back onto the grid when their own demand is low, especially during peak-pricing periods; (v) using standby or emergency power to backup grid-based power; (vi) improving customer power quality and reliability; (vii) serving niche applications, such as "green" power or remote power; and (viii) meeting continuous power, premium power, or cogeneration needs of the residential market.

### Customer Generation

Continuous customer generation applications produce power on a nearly continuous basis, running at least 6,000 hours per year. When evaluating the usage of DG technologies in this capacity, customers consider competing grid price, as well as the installed cost of the unit and fuel costs. Maintenance costs, power quality, and reliability of grid power are other critical components. In non-attainment areas, emissions can provide a strong barrier to these applications.

### Cogeneration

Cogeneration, also known as combined heat and power (CHP), utilizes otherwise wasted exhaust heat as useful thermal output, typically steam. The steam may be used either for space heating or space cooling. Again, CHP applications are driven by grid price and installed cost, but emissions can provide a strong barrier to implementation, especially in non-attainment areas. As with continuous power applications, these

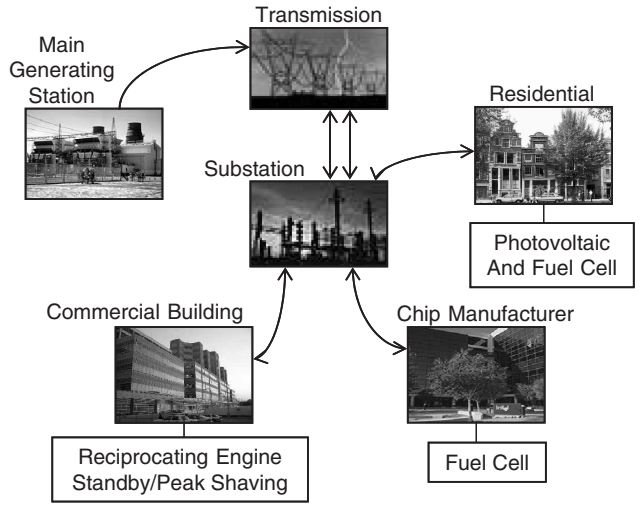


**FIGURE 28.1** Illustration of a DG-based power generation.

**TABLE 28.1** Attributes of commercially available and emerging DER technologies

| DER Technologies | Commercially Available | Emerging Technology | Size | Efficiency (%) |
|---|---|---|---|---|
| Microturbines | X | X | 10–300 kW | 20–30 |
| Reciprocating engines | X | – | 50 kW–6 MW | 33–37 |
| Stirling engines | – | X | 10–200 kW | <40 |
| Solid-oxide fuel cells (SOFC) | X | X | 5 kW–3 MW | 45–65 |
| Proton-exchange-membrane fuel cells | X | – | 1 kW–3 MW | 34–36 |
| Photovoltaic systems | X | – | 1 kW–1 MW | <22 |
| Wind systems | X | X | | <30 |
| Hybrid systems | – | X | <1 kW–1 MW | 40–50 |
| Combined heat and power (CHP) | X | X | 5 kW–25 MW | 50–80 |

units will run on a nearly continuous basis, typically at least 6,000 hours per year.

**Peak Shaving**

Driven primarily by high utility demand charges, peak-shaving applications (sometimes called peak clipping) are also affected by installed cost, perceived unit reliability, and fuel prices. These units operate much less frequently than do continuous power or CHP applications, often running as few as several hundred hours annually.

**Selling Power to the Grid under Net Metering**

Depending on what state they live in, some customers may be eligible for net metering. If eligible, net metering effectively allows a customer to sell its excess generation back to the grid at the same retail price as the customer buys power from the grid during other periods. With this financial incentive, the market for small commercial and residential DG installations, especially those based on the renewable energy technologies, should increase.

**Standby/Emergency Generation**

Applications providing standby or emergency power are typically driven by the reliability (perceived or real) of the grid and the cost to the customer of outage. Although the DG unit may only operate a few hours a year, it is used to power critical devices whose failure would result in property damage and/or threatened health and safety. Some customers like hospitals and airports may be required by code to install and maintain these units. For others, the high cost of outage drives the application. The choice of DG technologies for these emergency and standby applications is determined by installed cost, time required to start (i.e. black-start response), fuel access/storage, and size/weight of the unit.

**Premium Power**

On-site generation can improve both power quality and power reliability, especially when backed up with grid-based power. This application requires a DG technology that can operate continuously. In an era of both increasing power outages and rising demand for premium power, many businesses may install DG units to protect against the risk and cost of power outages. These customers include banks, semiconductor manufacturers, grocery stores, hospitals, and many other industrial and commercial market sites.

**Green Power**

Many of the renewable technologies and fuel cells have very low emissions. With the addition of emission-reducing technologies, microturbines and miniturbines also emit low levels of regulated gases. Customers, who are environmentally inclined, may purchase these DG applications for this reason, even if they have to pay a slight premium for green power compared with grid-based power purchases.

**Remote Power**

Residences and small commercial establishments (such as ranches, dairy farms, and flower growers) that are located well away from the transmission and distribution (T&D) system may prefer to generate their power on-site. By doing so, they eliminate both the cost of connecting to the grid and any problems associated with their position at the end of a long T&D line. The elimination of these problems, which include power outages and lower quality power, can produce the compelling economics necessary to the further use of DG technologies in a remote power capacity.

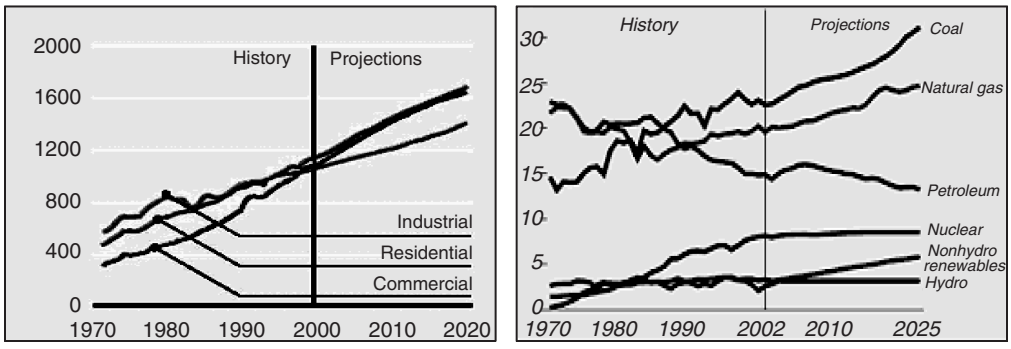


**FIGURE 28.2** (a) Current and projected electricity sales in terawatt-hours (TWh) by sector and (b) energy production (quadrillion BTU) by fuel in USA [3].

## 28.2 Fuel-cell Based Energy Systems for DG

Hydrogen-based fuel-cell[1] energy is one of the two front-runner alternative-energy solutions to address and alleviate the imminent and critical problems of rapid depletion of existing fossil-fuels (as illustrated in Fig. 28.2) and environmental pollution due to high emission. The framework for integrating these "zero-emission" alternative-energy sources to the existing energy infrastructure has been provided by the concept of DG, which provide an additional advantage: reduced reliance on existing and new centralized power generation, thereby saving significant capital cost. However, to achieve the projected worldwide target of $50 billion by 2015, the fuel-cell energy systems (as illustrated in Fig. 28.5) have to address cost, durability and reliability, and energy efficiency.

Currently, the applications of fuel cells (especially SOFC) for stationary applications are primarily for (i) lower power residential with a power range of $<5$ kW and (ii) for very high power reactive-power and harmonic compensations and high temperature coal-power applications. In Sections 28.3 and 28.4, we outline some established and possible power-electronic topologies for low- and high-power stationary applications, respectively.

[1]Table 28.1 shows that SOFC (electrical characteristics illustrated in Fig. 28.3) is the most energy efficient among the listed DG equipment. The efficiencies of the SOFC systems can be further enhanced by utilizing the quality of waste heat derived from the fuel-cell reactions for CHP and combined cycle applications (as illustrated in Fig. 28.4).

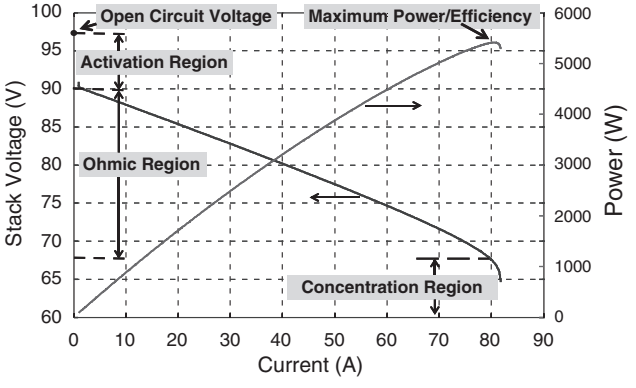


**FIGURE 28.3** Illustration of a SOFC operation in activation, ohmic, and concentration/mass-transport regions. The simulated current–voltage characteristics and the corresponding power output for a 100-cell planar SOFC stack are shown.

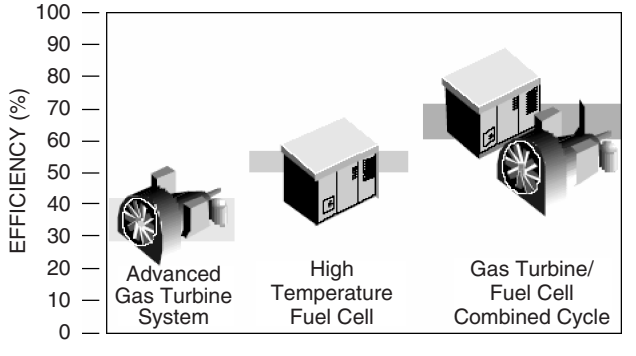


**FIGURE 28.4** An illustration showing the vision of combined SOFC and gas-turbine operation to improve energy efficiency.

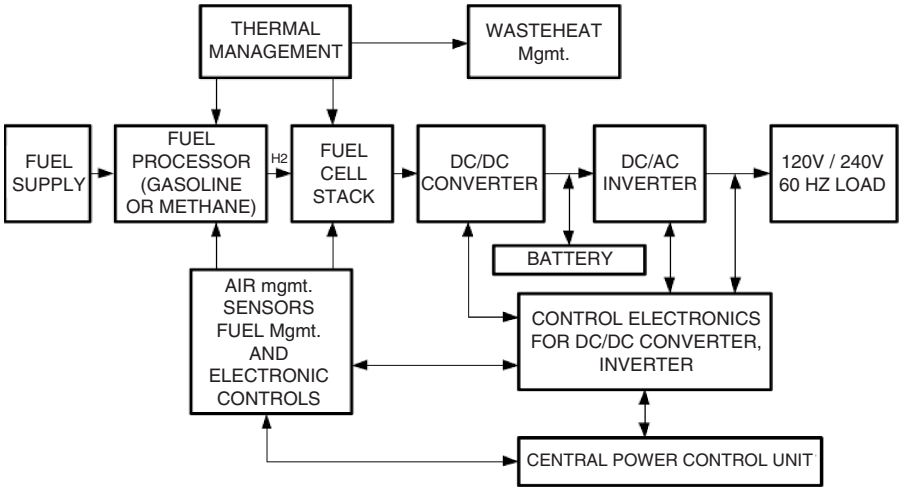


**FIGURE 28.5** A typical fuel-cell energy system architecture comprising: (a) the fuel processor/balance-of-plant (BOP); (b) the fuel-cell stack (see Fig. 28.3 for a typical characteristic); and (c) the power-electronic subsystem (PES). We note that single-stage PES design is also feasible.

## 28.3 Power-electronic Topologies for Residential Stationary Fuel-cell Energy Systems

The choice of power-electronic topologies can be broadly categorized as push–pull and full-bridge based topologies. In [4–7], low-cost push–pull topology for power levels >1 kW is proposed. Push–pull based topology, owing to its low part count, is a good candidate for a low-cost fuel-cell converter and can achieve an efficiency of 90% for low and medium power. However, at higher power it can suffer from transformer flux imbalance and core-saturation problems. For current-fed topologies, the main limitation is encountered at greater than 3 kW, where, leakage inductance of the transformer poses a problem, unless soft switching is used. Further, the limited available range of switch duty cycle also makes it difficult to track variations in the input voltage. In [8–14], full-bridge based fuel-cell inverter topologies are discussed. Because of the symmetrical transformer flux and equal electrical stress distribution, several variations of full-bridge inverter topologies have been found to be useful from the cost and efficiency point of view, especially when implemented for power levels greater than 3 kW. A 1.8 kW prototype of a boost converter followed by a two-stage dc/ac converter is discussed in [9]. The two-stage dc/ac converter comprises a full-bridge high-frequency inverter and a cycloconverter, both operating at the same switching frequency, is based on a novel multi-carrier pulse-width modulation (PWM). A similar two-stage dc/ac converter is discussed in [13], which incorporates a zero-current switched cycloconverter; while the full-bridge high-frequency inverter is switched with a fixed 50% duty cycle. An improved version of the prototype in [13], comprising a soft-switched sine-wave pulse-width modulation (SPWM) full-bridge HF inverter followed by a cycloconverter (operating at line frequency) is proposed in [14]. Among all the low-cost fuel-cell inverters [4–14], which aim to achieve an efficiency of greater than 90%, a maximum full-load efficiency of 87 and 89% is demonstrated in [4] and [14], respectively. Also, the power-electronic topologies in [4–14] are not designed to improve efficiency of the stack.

In this section, we describe three low-power stationary fuel-cell power-conversion schemes being pursued at the University of Illinois, Chicago with focus low cost, energy efficiency, and reliability. The first PES comprises a zero-ripple boost converter followed by a two-stage dc/ac converter comprising a soft-switched phase-shifted SPWM multilevel high-frequency inverter and a line-frequency-switched cycloconverter. The second PES comprises a front-end phase-shifted high-frequency full-bridge inverter followed by a step-up high-frequency transformer and a dual forced cycloconverter for universal power conditioning at high efficiency. The final PES comprises a single-stage isolated differential Ĉuk inverter [15] and has very low switch count and reduced cost.

### A. Ripple-mitigating Power Conditioner [16–18]

The power conditioner described in this section comprises a fuel-cell powered dc/dc zero-ripple boost converter (ZRBC), which generates a high voltage dc at its output, followed by a soft-switched, transformer isolated dc/ac inverter, which generates a 110 V ac. The high-frequency (HF) inverter switches are arranged in a multilevel fashion and are modulated by a fully rectified sine wave to create a HF, three-level ac voltage as shown in Fig. 28.6. Multilevel arrangement of the switches is particularly useful when the intermediate

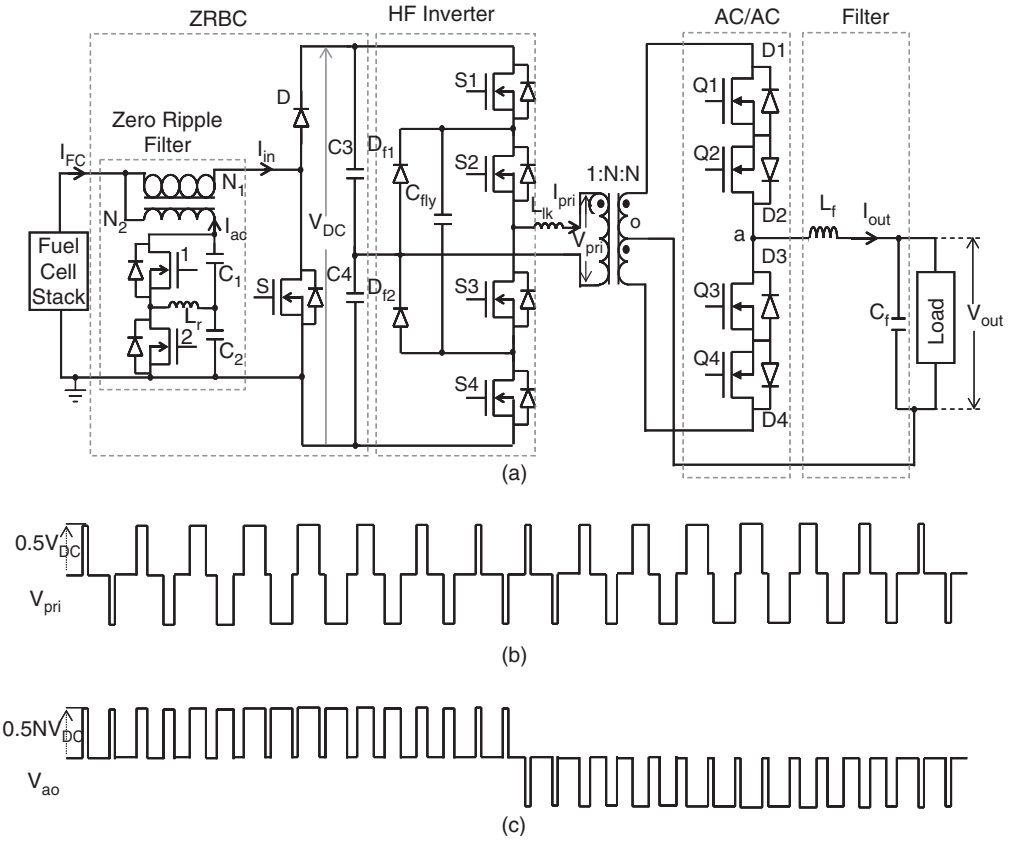


**FIGURE 28.6** Schematic of the ripple-mitigating fuel cell power conditioner [16–18].

dc voltage >500 V. The HF inverter is followed by the ac/ac cycloconverter which converts the three-level ac to a voltage that carries the line-frequency sinusoidal information.

**Zero Ripple Boost Converter (ZRBC)**

The ZRBC is a standard non-isolated boost converter, with the conventional inductor replaced by a hybrid zero-ripple filter (ZRF). The ZRF (shown in Fig. 28.6) is viewed as a combination of a coupled inductor (shown in Fig. 28.6) and a half-bridge active power filter (APF) (shown in Fig. 28.6). Such a hybrid structure serves the dual purpose of reducing the high- and the low-frequency current ripples. The coupled inductor minimizes the high-frequency ripple from the fuel-cell current ($I_{FC} + i_2 = i_1$) and the APF minimizes the low-frequency ripple from the fuel-cell current ($I_{FC} + i_{ac} = i_{in}$). $I_{FC}$ is the dc current supplied by the fuel cell, $i_2$ is the high-frequency ac current supplied by the series combination of identical capacitors $C_1$ and $C_2$ (in Fig. 28.6), and $i_{ac}$ is the low-frequency ac current supplied by the APF storage reactor $L_r$. For effective reduction of the high-frequency current from the fuel-cell output, the value of the capacitors $C_1$ and $C_2$ should be as large as possible. However, the series combination should be small enough to provide a high impedance path to the low-frequency current $i_{ac}$. Therefore, for a chosen value of capacitor, the values of the following expression hold true [18]:

$$C_1 = C_2 = 2C \tag{28.1a}$$

$$f_{HF} = \frac{1}{\sqrt{L_2 C}} \tag{28.1b}$$

$$f_{LF} = \frac{1}{\sqrt{4L_r C}} \tag{28.1c}$$

where

$f_{HF}$ is the switching frequency of the converter,

$f_{LF}$ is the lowest frequency component in $i_{ac}$.

Assuming the switching frequency is approximately twenty times the lowest frequency component, the value of ZRF

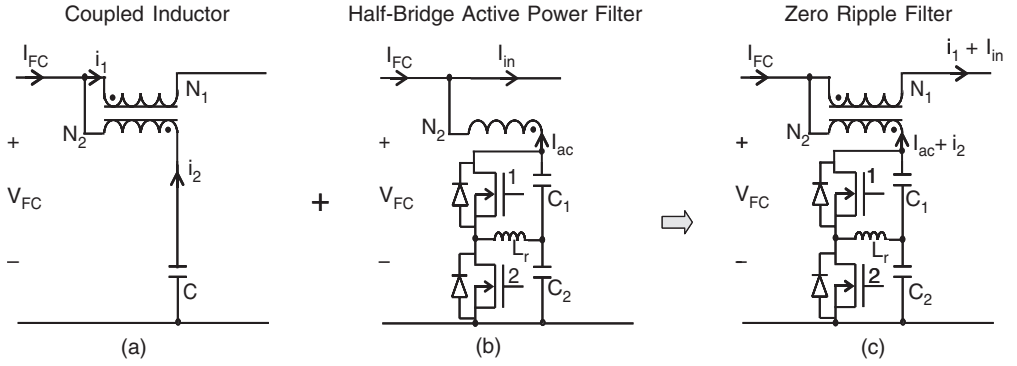


**FIGURE 28.7** Schematic diagrams for: (a) coupled-inductor structure for reducing the HF current ripple; (b) half-bridge active filter, which compensates for the low frequency harmonic current ripple demand by the inverter; and (c) the proposed hybrid zero ripple filter structure.

passive components $L_2$ and $L_r$ can be determined as follows [18]:

$$f_{HF} \geq 20 f_{LF} \tag{28.1d}$$

$$\frac{1}{\sqrt{L_2 C}} \geq \frac{10}{\sqrt{L_r C}} \tag{28.1e}$$

$$L_r \geq 100 L_2 \tag{28.1f}$$

Therefore, the value of $L_2$ should be small in order to limit the value of $L_r$ and also to minimize the phase shift in the injected low frequency current $i_{ac}$.

In the following sub-sections, the high- and low-frequency ac-current reduction mechanisms (Fig. 28.7) and the conditions to achieve it are discussed. In addition to this, the effect of coupled inductor parameters on the bandwidth of the open loop system will be discussed. For the purpose of analysis, the value of the capacitors $C_1$ and $C_2$ are assumed to be large. Hence, the dynamics of the APF is assumed to have minimal effect on the coupled inductor analysis.

**High-frequency Current-ripple Reduction**

In this section, the inductance offered by the coupled inductor and the ripple reduction achievable is discussed. For that purpose we need to derive an expression for the effective inductance of the coupled inductor. Because, the value of the capacitors $C_1$ and $C_2$ are large and that of $L_{22}$ is small, the dynamics of the APF is assumed to have minimal effect on the coupled-inductor analysis. In the pi-model for the zero ripple coupled inductor and the excitation voltage and the current for the primary and the secondary windings are shown in the Fig. 28.8. The currents $i_{1HF}$ and $i_{2HF}$ are, respectively, the primary and the secondary AC currents shown in Fig. 28.8.

$$v_{FC} = (L_1 + L_M)\frac{di_{1HF}}{dt} + nL_M\frac{di_{2HF}}{dt} \tag{28.2a}$$

$$v_C = (L_1 + L_M)\frac{di_{1HF}}{dt} + (L_2 + nL_M)\frac{di_{2HF}}{dt} \tag{28.2b}$$

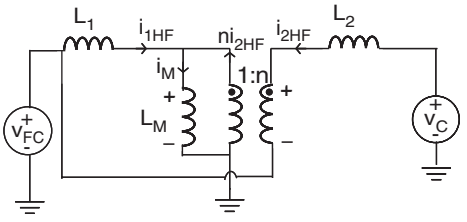


**FIGURE 28.8** AC model for the coupled inductor shown in Fig. 28.7a.

$$n = \frac{N_2}{N_1} \cong \sqrt{\frac{L_{22}}{L_{11}}} \tag{28.2c}$$

where $L_{11}$ is the self inductance of the primary winding with $N_1$ turns. Solving Eqs. (28.2a and b), the expressions for $di_{1HF}/dt$ and $di_{2HF}/dt$ are obtained using

$$\frac{di_{1HF}}{dt} = \frac{(L_2 + nL_M)v_{FC} - nL_M v_C}{(L_1 + L_M)L_2} = \frac{v_{FC}}{L_1 + L_M} + \frac{nL_M(v_{FC} - v_C)}{(L_1 + L_M)L_2} \tag{28.3a}$$

$$\frac{di_{2HF}}{dt} = \frac{v_{FC} - v_C}{-L_2} \tag{28.3b}$$

By substituting Eq. (28.3a) in (28.3b), we obtain the following expression:

$$\frac{di_{1HF}}{dt} = \frac{(L_2 + nL_M)v_{FC} - nL_M v_C}{(L_1 + L_M)L_2} = \frac{v_{FC}}{L_1 + L_M} + \frac{nL_M}{(L_1 + L_M)}\frac{di_{2HF}}{dt} \tag{28.3c}$$

To reduce the AC component of the fuel-cell-stack current to zero, the following condition should hold true:

$$\frac{di_{1HF}}{dt} = \frac{di_{2HF}}{dt} \tag{28.4}$$

Therefore, using the above condition and Eq. (28.3c), we obtain

$$\frac{di_{1HF}}{dt} = \frac{v_{FC}}{L_{11}\left[1 + \frac{(1+n)}{n}k\right]} = \frac{V_{FC}}{L_{eff}} \tag{28.5}$$

The denominator of Eq. (28.5) is the effective inductance $L_{eff}$ offered by the coupled-inductor structure of the hybrid filter. The effective inductance depends on the turns ratio $n$, the coupling coefficient $k$, and the self inductance $L_{11}$ of the primary winding. For very small values of turns ratio ($n \ll 1$), significantly large values of effective inductances can be obtained. Figure 28.9 shows the effective inductance curves and the corresponding reduction in the ripple. Figure 28.9a shows the dependence of normalized $L_{eff}$ on $n$ as a function of $k$. For the values of effective inductance shown in Fig. 28.9a, the corresponding values of achievable ripple current in both the coupled-inductor windings are shown in Fig. 28.9b. Using Fig. 28.9b, a designer can decide on a value of high-frequency current ripple and using the corresponding values of $n$ and $k$, the normalized effective inductance can be chosen from Fig. 28.9a. While deciding the value of high-frequency ripple, one should choose a small value for $n$ (<0.25), to ensure that $L_{22}$ is small enough to prevent significant variations in the voltage across capacitors $C_1$ and $C_2$. Also, the effective inductance should be chosen to meet the bandwidth requirements of the ZRBC. Increase in the effective input inductance has a two-pronged effect on the open loop frequency response of the ZRBC. First, the bandwidth is reduced and second, the RHP zero is drawn closer to the imaginary axis, resulting in a reduction in the available phase margin and thereby the ZRBC stability.

**Active Power Filter**

The input current of the inverter comprises as dc component and a 120 Hz ac component and is expressed as

$$I_{dc} + I_{ac} = \frac{V_{out}I_{out}}{V_{dc}}\cos(\theta) - \frac{V_{out}I_{out}}{V_{dc}}\cos(2\omega t - \theta) \tag{28.6}$$

where

$V_{out}$ inverter output voltage,
$I_{out}$ are inverter output current,
$V_{dc}$ is the average value of voltage across the series capacitors $C_1$ and $C_2$,
$\theta$ is the load power factor angle.

Here, we derive the condition for low frequency current ripple elimination from the PCS input current. For the APF shown in Fig. 28.6, the voltage across the storage reactor $L_r$ of the APF is expressed as

$$V_{ab} = V_a - \frac{V_{dc}}{2} = V_{dc}\left(S_a - \frac{1}{2}\right) \tag{28.7}$$

where $S_a$ is the modulating signal. The reactor current $i_r$ is

$$i_r = \frac{V_{dc}(S_a - 1/2)}{j\omega L_r} \tag{28.8}$$

where

$$S_a = 0.5 + \sum_{n=1}^{\infty} B_n \sin n(\omega t + \phi)$$

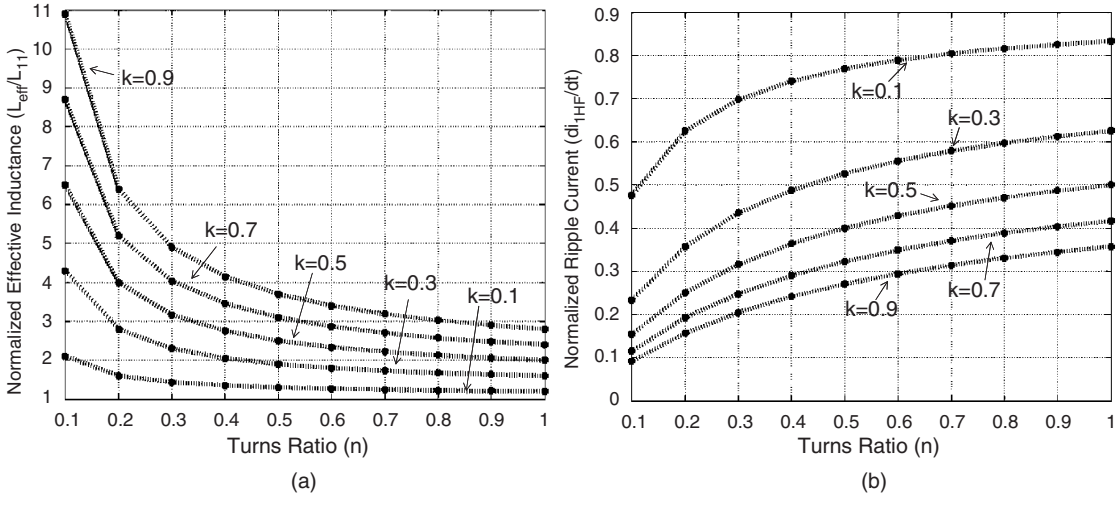


**FIGURE 28.9** Normalized: (a) effective inductance and (b) ripple current of the coupled inductor.

$$i_r = \frac{V_{dc}}{\omega L_r} B_n \sin\left(\omega t + \phi - \frac{\pi}{2}\right) \quad \text{(considering only the fundamental component)}$$

The current injected by the APF is

$$i_{ac} = (S_a - \frac{1}{2}) i_r \tag{28.9a}$$

$$i_{ac} = \frac{V_{dc}}{\omega L_r} B_n^2 \sin(\omega t + \phi) \sin\left(\omega t + \phi - \frac{\pi}{2}\right) \tag{28.9b}$$

$$i_{ac} = \frac{V_{dc}}{2\omega L_r} B_n^2 \left[\cos\left(\frac{\pi}{2}\right) - \cos\left(2\omega t + 2\phi - \frac{\pi}{2}\right)\right] \tag{28.9c}$$

In order to reduce the 2nd harmonic in the input current to zero, $i_{ac} = I_{ac}$

$$\frac{V_{dc}}{2\omega L_r} B_n^2 \left[\cos\left(2\omega t + 2\phi - \frac{\pi}{2}\right)\right] = \frac{V_o I_o}{V_{dc}} \cos(2\omega t - \theta) \tag{28.10a}$$

which yields

$$B_n = \frac{\sqrt{2\omega L_r V_o I_o}}{V_{dc}} \tag{28.10b}$$

$$\phi = \frac{\pi}{4} - \frac{\theta}{2} \tag{28.10c}$$

**DC/AC Converter**

A two-stage dc/ac converter (shown in Fig. 28.10) comprises a soft-switched phase-shifted synchronized pulse-width modulation (SPWM) multilevel HF inverter and a line-frequency switched ac/ac cycloconverter. The multilevel arrangement of the HF inverter switches reduces the voltage stress and the cost of the high-frequency semiconductor switches. The ac/ac stage comprises a single-phase cycloconverter and an output LC filter. The cycloconverter has two bidirectional switch pairs $Q_1$ and $Q_2$ and $Q_3$ and $Q_4$ for a single-phase output. In order to achieve a 60-Hz sine-wave ac at the output, the sine wave modulation can be performed either on the HF inverter or on the cycloconverter. Therefore, two different modulation strategies are possible for the dc/ac inverter. Both schemes result in the soft switching of the HF inverter while the cycloconverter is hard switched.

In the first modulation scheme the cycloconverter switches follow SPWM, while the HF inverter switches are switched at fixed 50% duty pulse. The HF inverter switches in this scheme undergo zero-voltage turn-on. In the second modulation scheme, the switches of the multilevel HF inverter follow SPWM and the cycloconverter switches are switched based on the power-flow information. Unlike the first modulation scheme, which modulates the cycloconverter switches at high frequency, in the second modulation scheme, cycloconverter operates at line frequency. The switches are commutated at high frequency only when the polarities of output current and voltage are different. Usually this duration is very small and therefore, the switching loss of the ac/ac cycloconverter is considerably reduced compared to the conventional control method. Therefore, the heat-sinking requirement of the cycloconverter switches is significantly reduced. The HF inverter switches in this scheme undergo zero-current turn-off. Control signals for the second modulation scheme are shown in Fig. 28.10.

**B. Universal Power Conditioner [19][2]**

This approach achieves a direct power conversion and does not require any intermediate energy storage components. As shown in Fig. 28.11, the final approach has a HF inverter followed by a HF transformer and a forced cycloconverter. Switches (Q1–Q4) on the primary of the HF transformer are sine-wave modulated to create a HF three-level ac voltage. The three-level ac at the output of the HF transformer is converted to 60/50 Hz line-frequency ac by the cycloconverter and the LC filter. For an input of 30 V, the transformation ratio of the HF transformer is calculated to be $N = 13$. Fabrication of a 1:13 transformer is relatively difficult. Furthermore, high turns ratio yields enhanced secondary leakage inductance and secondary winding resistance, which result in measurable loss of duty cycle and secondary copper losses, respectively. Higher leakage also leads to the higher voltage spike, which added to the high nominal voltage of the secondary that necessitate the use of high-voltage power devices. Such devices have higher on-resistance and slower switching speeds.

Therefore, a combination of two transformers and two cycloconverters on the secondary side of the HF transformer is identified to be an optimum solution. For an input voltage in the range of 30–42 V, we use $N = 6.5$, while for an input voltage above 42 V, we use $N = 4.3$. To change the transformation ratio of the HF transformer, we use a single-pole-double-throw (SPDT) relay, as shown in Figs. 28.11a, b. Such an arrangement not only improves the efficiency of the transformer but also significantly improves the utilization of the cycloconverter switches for operation at 120/240 V ac and 60/50 Hz. For 120 V ac output, the two cycloconverter filter capacitors are paralleled (as shown in Fig. 28.11a) while for 240 V ac output, the voltage of the filter capacitor are connected in opposition (as shown in Fig. 28.11b).

**Modes of Operation**

In this section, we discuss the modes of operation of the inverter in Fig. 28.11 for 120 V ac output and for an input voltage in the range of 42–60 V (i.e. $N = 4.3$). The modes of operation below 42 V (i.e. $N = 6.5$) remains the same.

[2]University of Illinois, Chicago secured the first position among U.S.A and 3rd position among worldwide university competition for this topology, which was developed as a part of 2005 IEEE Future Energy Challenge Competition.

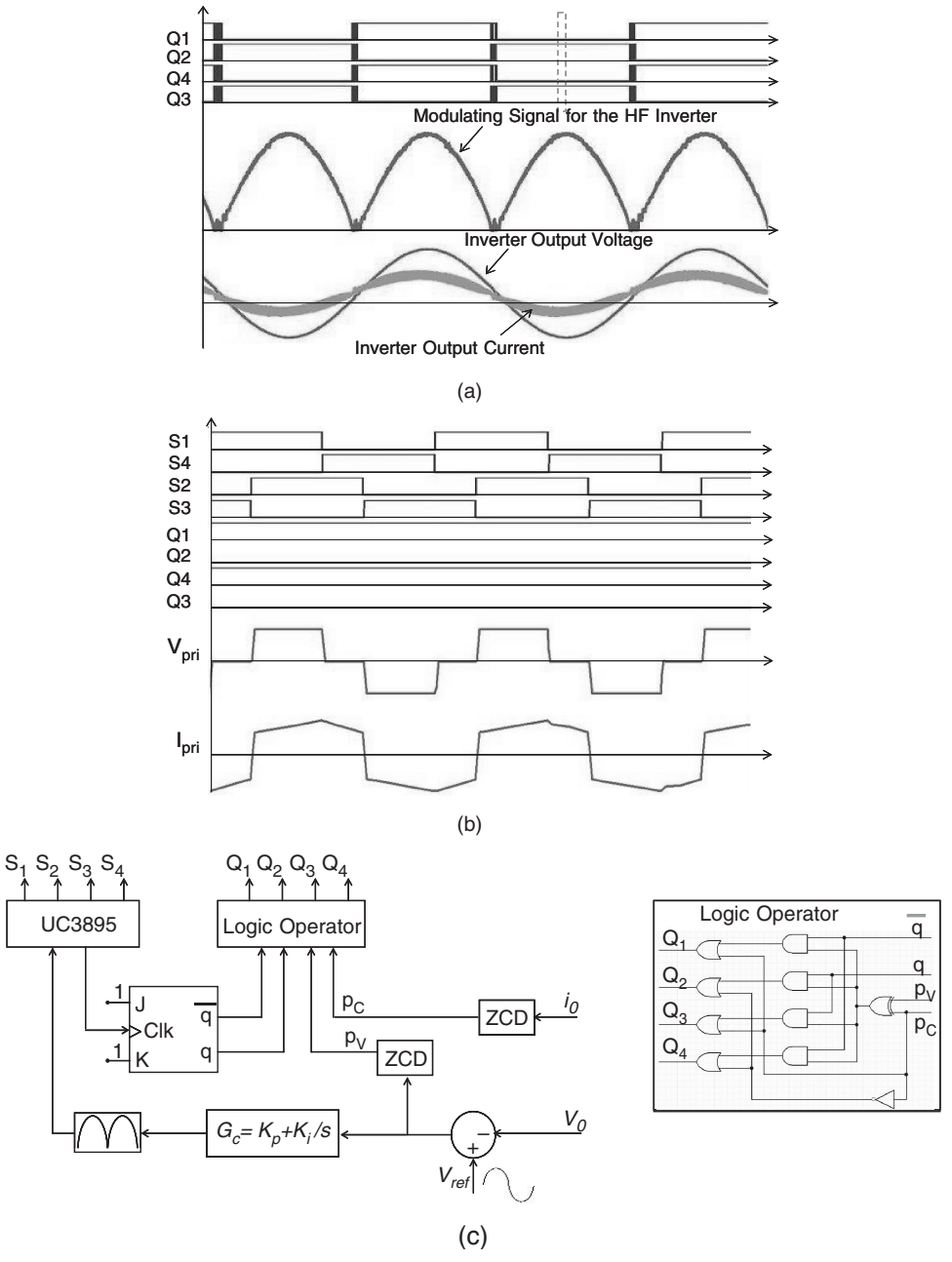


**FIGURE 28.10** (a) Schematic waveforms for the inverter operation; (b) schematic waveforms for the HF inverter; and (c) overall control scheme for the HF inverter.

Figure 28.10 shows the waveforms of the five operating modes of the phase-shifted HF inverter and a positive primary and a positive filter-inductor current. Modes 2 and 4 show the zero-voltage switching (ZVS) turn-on mechanism for switches $Q_3$ and $Q_4$, respectively. Unlike conventional control scheme for cycloconverter [13], which modulates the switches at high frequency, the proposed cycloconverter operates at line frequency. The switches are commutated at high frequency only when the polarities of the output current and voltage are different [13]. For unity power-factor operation, this duration is negligibly small and therefore, the switching loss of the ac/ac cycloconverter is considerably reduced compared to the conventional control method [14, 16].

*Five modes of the PES operation are discussed for positive primary current. A set of 5 modes exists for a negative primary current as well. A similar set of five modes of operation for the 240 V ac exists [19] for input voltage above 42 V ($N = 4.5$).*

Again, the mode of operation for input voltage below 42 V ($N = 6.5$) remains the same.

**Mode 1** (Fig. 28.12a): During this mode, switches $Q_1$ and $Q_2$ of the HF inverter are on and the transformer primary current $I_{p1}$ and $I_{p2}$ is positive. The load current splits equally between the two cycloconverter modules. For the top cycloconverter module, the load current $I_{out}/2$ is positive and flows through the switches pair $S_1$ and $S_1'$, the output filter $L_{f1}$ and $C_{f1}$, switches $S_2$ and $S_2'$, and the transformer secondary. Similarly, for the bottom cycloconverter module, the load current

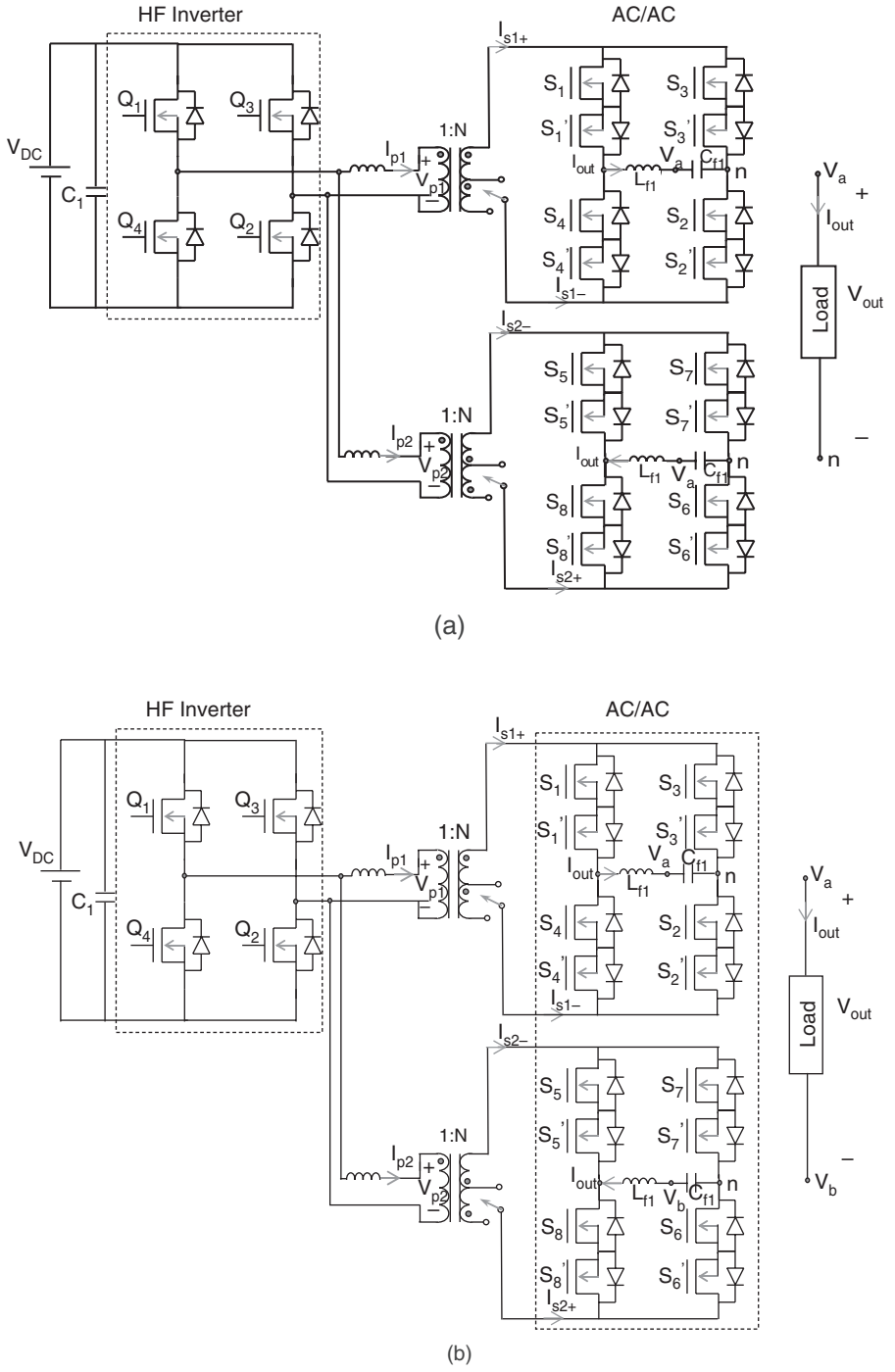


**FIGURE 28.11** (a) and (b) Schematics for converter operation, respectively, at 120 V ac and 60 Hz and 240 V ac and 50 Hz; (c) and (d) control schemes of the power electronic system (PES) in stand-alone and grid-connected modes [19].

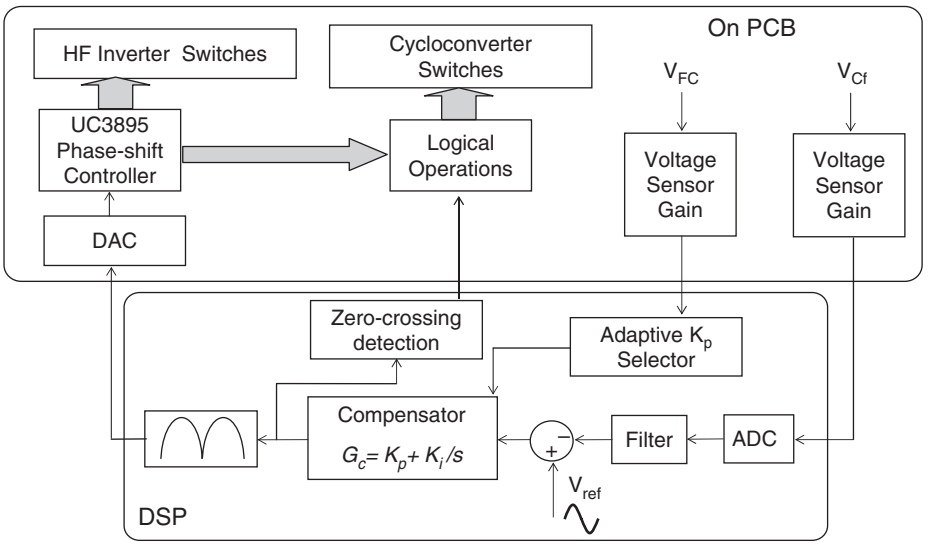


(c)

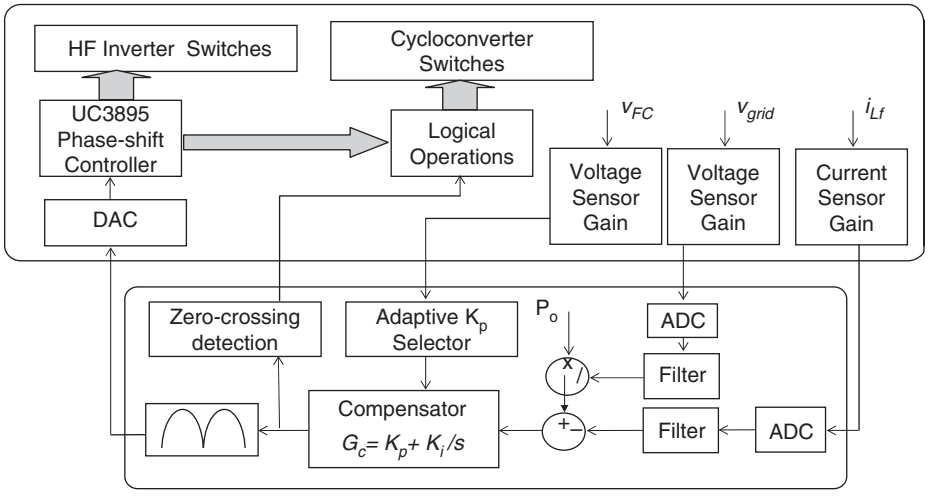


(d)

**FIGURE 28.11** *continued*

$0.5 \times I_{out}$ is positive and flows through the switches pair $S_5$ and $S_5'$, the output filter $L_{f2}$ and $C_{f2}$, switches $S_6$ and $S_6'$, and the transformer secondary.

**Mode 2** (Fig. 28.12b): At the beginning of this interval the gate voltage of the switch $Q_1$ undergoes a high-to-low transition. As a result, the output capacitance of $Q_1$ begins to accumulate charge and at the same time the output capacitance of switch $Q_4$ begins to discharge. Once the voltage across $Q_4$ goes to zero, it is can be turned on under ZVS. The transformer primary currents $I_{p1}$ and $I_{p2}$ and the load current $I_{out}$ continue to flow in the same direction. This mode ends, when the switch $Q_1$ is completely turned off and its output capacitance is charged to $V_{DC}$.

**Mode 3** (Fig. 28.12c): This mode initiates when $Q_1$ turns off. The transformer primary currents $I_{p1}$ and $I_{p2}$ are still positive, and freewheels through $Q_4$ as shown in Fig. 28.12c. Also the load current continues to flow in the same direction as in Mode 2. Mode 3 ends at the commencement of turn off $Q_2$.

**Mode 4** (Fig. 28.12d): At the beginning of this interval, the gate voltage of $Q_2$ undergoes a high-to-low transition. As a result of this, the output capacitance of $Q_2$ begins to accumulate charge and at the same time, the output capacitance of switch $Q_3$ begins to discharge as shown in the Fig. 28.12d. The charging current of $Q_2$ and the discharging current of $Q_3$ together add up to the primary current $I_{p1}$ and $I_{p2}$.

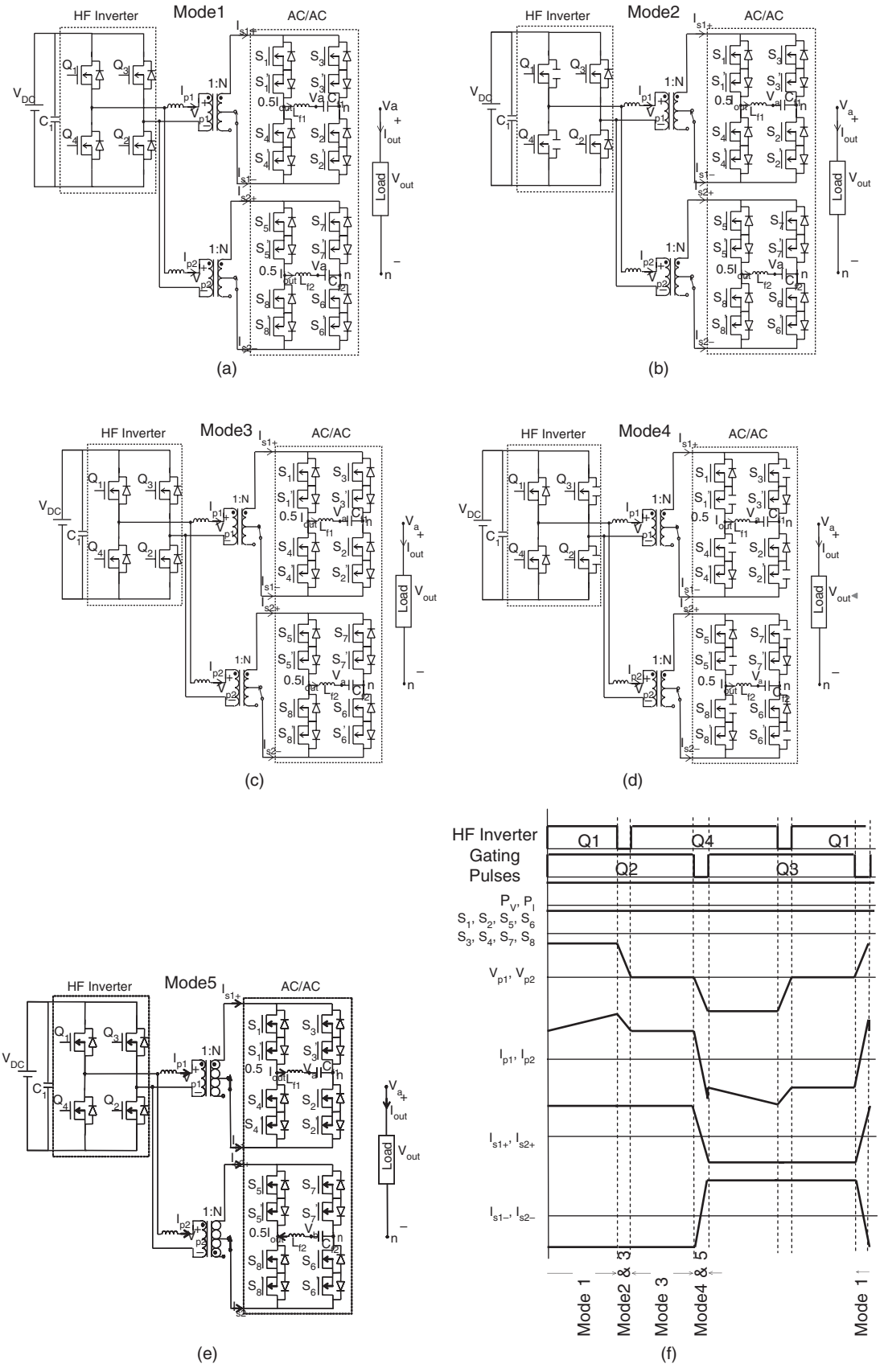


**FIGURE 28.12** Modes of operation for 120 V ac for input voltage in the range of 42–60 V ($N = 4.3$): (a–e) topologies corresponding to the five operating modes of the overall dc/ac converter for positive primary current and for power flow from the input to the load and (f) schematic waveforms show the operating modes of the HF inverter when primary currents are positive. *The modes of operation below 42 V (i.e. $N = 6.5$) remains the same.*

The transformer current makes a transition from positive to negative. Once the voltage across $Q_3$ goes to zero, it is turned on under ZVS. The load current flows in the same direction as in Mode 3, but makes a rapid transition from the bidirectional switches $S_1$ and $S_1'$ and $S_2$ and $S_2'$ to $S_3$ and $S_3'$ and $S_4$ and $S_4'$ and during this process $I_{out}/2$ splits between the two legs of the cycloconverter modules as shown in Fig. 28.12d. Mode 4 ends when the switch $Q_2$ is completely turned off and its output capacitance is charged to $V_{DC}$. At this point, it is necessary to note that since $S_1$ and $S_2$ are off simultaneously, each of them support a voltage of $V_{DC}$.

**Mode 5** (Fig. 28.12e): This mode starts when $Q_2$ is completely turned off. The primary current $I_{p1}$ and $I_{p2}$ is negative, while the load current is positive as shown in Fig. 28.12e.

### C. Low-cost Fuel-cell Power Conditioner

Low cost power electronics system (PES) that converts a fuel cell stack's low voltage (typically 30–60 V) output into a commercial ac output is critical for the success of fuel-cell energy system, especially for the low power applications ($\leq$3 kW). According to [20], the cost of stationary residential PES should be less than \$40/kW for high volume of production. Many types of configurations have been tried to achieve fuel-cell power conversion at lower cost without compromising efficiency [5, 7, 11–13, 19, 21–23]. Based on where the transformer is inserted for isolating the fuel cell from the load, they can be broadly categorized into two types of topologies.

The first type, usually called "dc/dc type converter," uses a dc/dc at front end to boost the low input voltage. The transformer is inserted into the dc/dc stage which usually is a push–pull or full-bridge converter. A diode rectifier is required at the secondary to obtain a higher dc voltage. Following the dc/dc stage, a non-isolated dc/ac stage is used to get low frequency ac. Since this type of topology has three power conversion stages (dc-high frequency ac–dc-low frequency ac), it may not be the best choice from efficiency and cost point of view because each stage has to have a very high efficiency to make the overall efficiency high, and usually more than six active components (switches and diodes) are required.

The second type of topology, referred as "cycloconverter type converter," reduce the system complexity by removing the dc/dc stage. The galvanic isolation is achieved by embedding the transformer into a dc/ac converter which usually composes of a three-level or full-bridge inverter followed by a cycloconverter. Although it has lesser power conversion stage, the number of active components may not necessary be less than that of the first type mainly due to the bidirectional switches, which are required for the cycloconverter.

A single-stage isolated dc/ac inverter, which was originally proposed in [15] as "push–pull amplifier" achieves direct dc/ac conversion by connecting load differentially across two bidirectional dc/dc Cuk converters and modulating them sinusoidally with 180° phase difference (Fig. 28.13). Since only four main switches are used, it would potentially reduce system complexity, costs, improve reliability, and increase efficiency. Furthermore, the common source connection between two devices both at primary and secondary sides ($Q_a$ and $Q_c$ and $Q_b$ and $Q_d$ in Fig. 28.13) makes the gate drive circuit relatively simple. In addition, the possibility of coupling inductors or integrated magnetics [24] will further reduce the overall volume and weight thereby achieving lesser material and space usage. Therefore, it would be a better alternative for fuel-cell application and will eventually lead to a very low cost, high density power conversion system.

Another advantage of this inverter is the reduction of turns ratio of the step-up transformer, which is usually required to achieve rated ac from low fuel-cell stacks dc voltage. The inherent voltage boosting capability of the dc/ac Cuk inverter can reduce the transformer turns ratio requirement by at least half. Low transformer turns ratio yields less leakage inductance

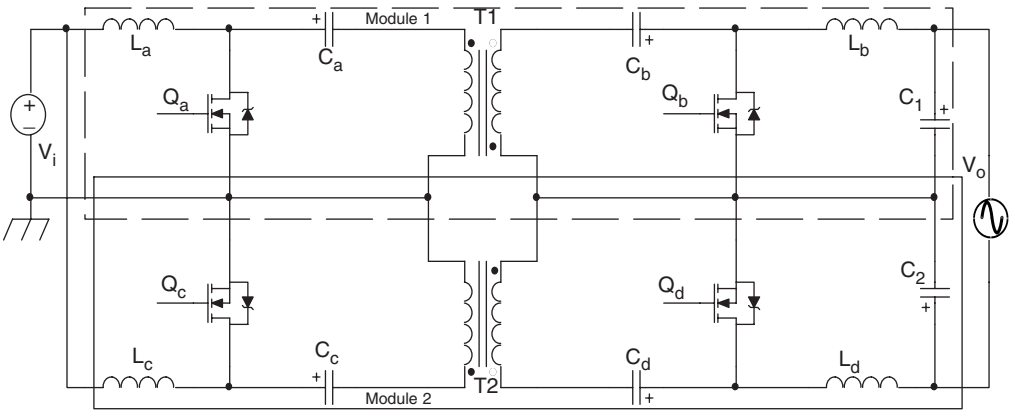


**FIGURE 28.13** Schematic of the single-stage dc/ac differential isolated Ĉuk inverter.

and secondary winding resistance, which reduces the loss of duty cycle and secondary copper losses, respectively.

Although the non-isolated dc/ac inverter has already been proposed [15], analysis of the isolated version has not appeared in any literature, nor have the issues involved in the design towards higher power rating (>1 kW) for fuel-cell application. Reference [25] presents the analysis and design of a 1 kW fuel cell PES using the isolated differential Cuk inverter.

The output of the proposed dc/ac inverter is the difference between two "sine-wave modulated PWM controlled" isolated Cuk inverter (module 1 and module 2), with their primary sides connected in parallel. The two diagonal switches of two modules are triggered by a same signal ($Q_a = Q_d$, $Q_b = Q_c$), while the two switches in each module have complementary gate signals ($Q_a = /Q_b$, $Q_c = /Q_d$). As we know, the output voltage of an isolated Cuk inverter can be expressed as

$$V_o = V_i \cdot \frac{D}{N(1-D)} \tag{28.11}$$

where $D$ is the duty ratio, $N$ is the transformer turns ratio, $V_i$ is the input voltage. Since duty ratios for module 1 and module 2 are complementary, the output difference between two modules is:

$$V_o = V\mathrm{c1} - V\mathrm{c2} = V_i \cdot \left[\frac{D}{\mathrm{N}\cdot(1-D)} - \frac{1-D}{N\cdot D}\right] \tag{28.12}$$

The curves corresponding to the terms in Eq. (28.12) with respect to the duty ratio $D$ (assuming $N = 1$) are plotted in Fig. 28.14. The figure shows that although the gain-duty ratio curves of modules 1 and 2 are not linear, their difference is almost linear. Therefore, if a sine-wave modulated duty ratio $D$ is used as a control signal for inverter in Fig. 28.13, its output voltage will be a sine wave with small distortion [15].

In order to understand how the current flows and energy transfers during the switching and to help select the device rating, four different modes of the inverter are analyzed and shown in Fig. 28.15. Figures 28.15a, b show the direction of the current when the load current flows from top to the bottom.

**Mode 1:** Figure 28.15a shows the current flow for the case when switch $Q_a$, $Q_d$ are ON and $Q_b$, $Q_c$ are OFF. During this time, the current flowing through the input inductor $L_a$ increases and the inductor stores energy. At the same time, the capacitor $C_a$ discharges through $Q_a$, and thus, there is transfer of energy from primary side to the secondary side through the transformer $T_1$. The capacitor $C_b$ is discharged to the circuit formed by $L_b$, $C_1$, and the load $R$. Meanwhile, the inductor $L_d$ stores energy and its current increases. The capacitor $C_d$ discharges through $Q_d$. The power flows in opposite direction in the module 2 from secondary to the primary side. The capacitor $C_c$ is also discharged to provide the power.

**Mode 2:** When $Q_a$, $Q_d$ are turned off, and $Q_b$, $Q_c$ are ON (Fig. 28.15b) $C_a$, $C_d$ and $C_b$, $C_c$ are charged using the energy, which was stored in the inductors $L_a$ and $L_d$ while $Q_a$, $Q_d$ were on. During this time, $L_b$ and $L_c$ will release their energy.

Figures 28.15c, d show the current direction when the load current flows in the opposite direction. The description for these two modes is omitted due to the similarity with Figs. 28.15a, b.

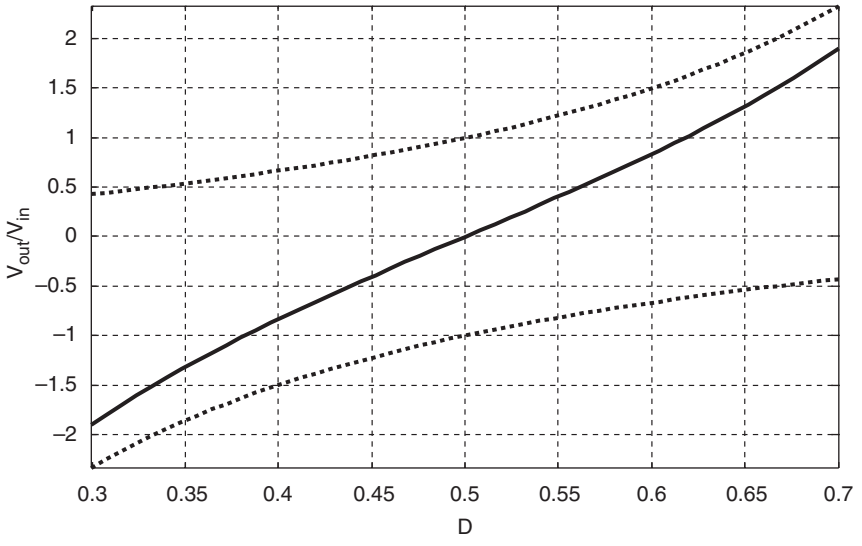


**FIGURE 28.14** Voltage gain vs $D$ for module 1 (top), module 2 (bottom), and their difference (middle).

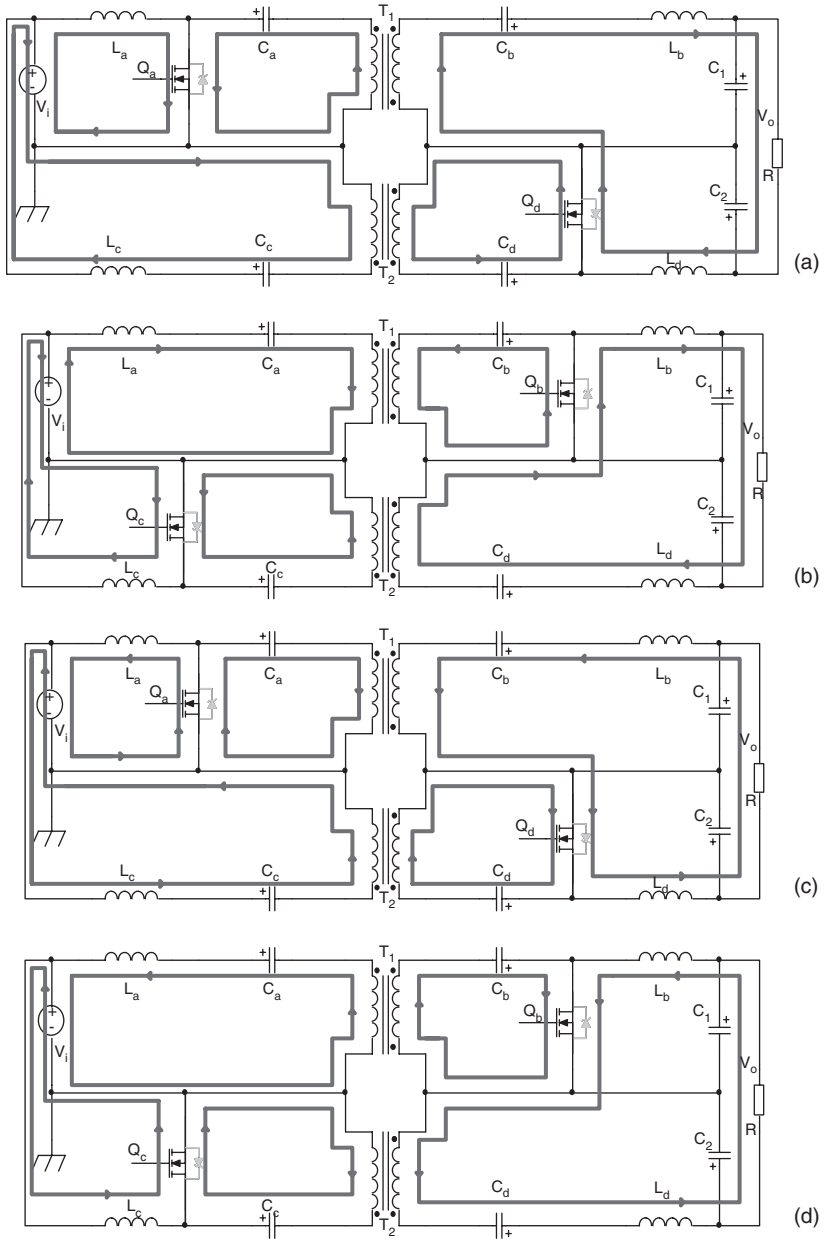


**FIGURE 28.15** (a) and (b) Direction of the current flow in two modes of operation for positive load current: (a) Mode 1, when $Q_a$, $Q_d$ are ON, $Q_b$, $Q_c$ are OFF and (b) Mode 2 when $Q_a$, $Q_d$ are OFF $Q_b$, $Q_c$ are ON. Figures 28.15c, d are the corresponding current flow when load current flows in the opposite direction.

## 28.4 Towards Power-electronic Topologies for High Power Fuel-cell Based DG

In addition to residential use, fuel cells are being increasingly considered for high-power (MW-power) applications. In that context, currently, Department of Energy's (DOEs) focus is on reactive-power and harmonic compensations and high-temperature coal-power applications. Due to the practical manufacture limitation and reliability concern, the maximal output voltage and output power of one fuel-cell stack cannot be too high. To provide the desired amount of voltage and/or power, multiple fuel-cell stacks are required to form a fuel-cell module. These modules along with their power conditioning system can be connected in several different configurations, which will be presented in this section.

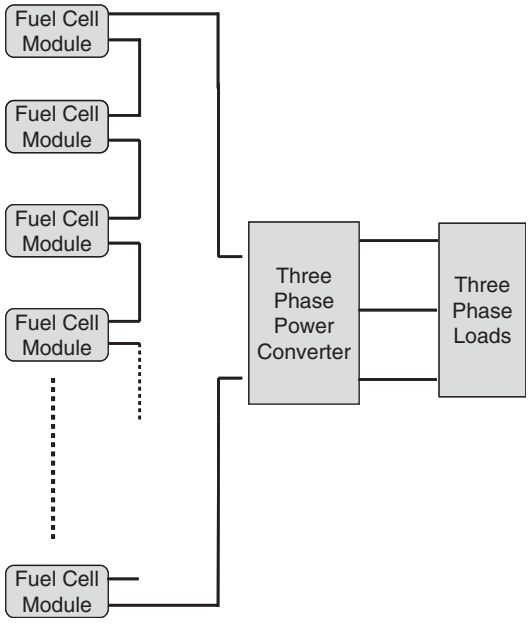


**FIGURE 28.16** A general diagram of multiple fuel-cell modules connected in series to generate dc bus followed by a three-phase inverter. Copyright © IEEE, 2003, Ozpineci etc. [26].

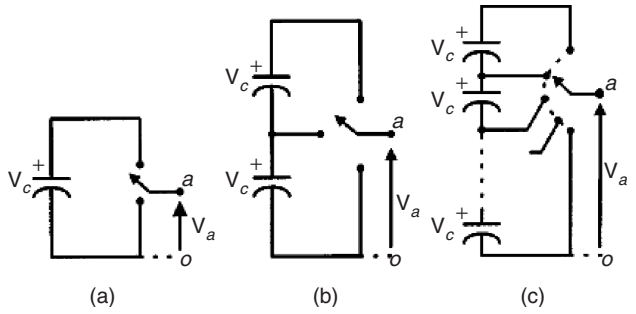


**FIGURE 28.17** One phase multilevel diagram: (a) two levels; (b) three levels; and (c) n-levels. Copyright © IEEE, 2002, Rodriguez etc. [27].

The advantages and disadvantages of each approach are also summarized.

One of the most common configurations of fuel-cell modules and PCS for high power application is to connect multiple fuel-cell modules directly in series and apply the obtained dc bus to a three-phase dc/ac inverter, as shown in Fig. 28.16. For each module, fuel-cell stacks can also be connected in parallel to provide the required power, if necessary.

For the inverter, recently, multilevel power conversion has received increasing attention for medium-voltage and high power applications. Among the multilevel topologies, diode-clamped inverter, capacitor-clamped (flying capacitor) inverter, and cascaded multi-cell inverter with separate dc sources are the three basic architectures. Other emerging novel topologies include asymmetric hybrid cells and soft-switched multilevel inverters [27].

Multilevel inverters include an array of power semiconductor devices and voltage sources. They generate output voltage with stepped waveforms. Figure 28.17 shows a schematic diagram of one phase leg multilevel converter with different number of levels. Note the actual power devices are replaced by ideal switches with several positions. Figure 28.17a is a two-level inverter since the output voltage $V_a$ has only two possible values, while Fig. 28.17b is a three-level inverter since its output can have three different values. If $m$ is the number of possible output voltage levels, it is called $m$-level inverter (Fig. 28.17c). By increasing the number of levels, the output voltage waveforms will have more steps and thus have a reduced harmonic distortion. However, a high number of levels will increase the complexity and introduce voltage imbalance problems.

Figure 28.18 show the diagrams of one phase leg fuel-cell power conditioner for high power applications using diode-clamped multilevel inverter. Its operational principle was explained in [27]. The number of switches equals $2 \times (m-1)$. The key components that make the circuit different are clamp diodes, which clamp the switch voltage to the corresponding level of the dc bus voltage. Assuming all the clamp diodes are the same, the number of diodes required for each leg will be $(m-1) \times (m-2)$. This represents a quadratic increase in $m$ (number of levels). Another problem caused by diode clamping is if the inverter operates under high frequency, the diode reverse recovery will become a major design challenges.

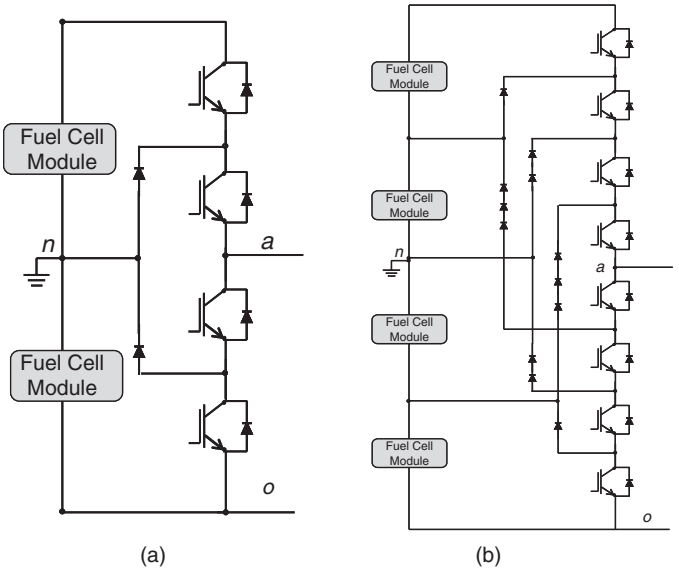


**FIGURE 28.18** Schematics of one phase leg fuel-cell power conditioner for high power applications using diode-clamped multilevel inverter: (a) three-level and (b) five-level inverter. Copyright © IEEE 2002, Rodriguez etc. [27] and 2003, Ozpineci etc. [26].

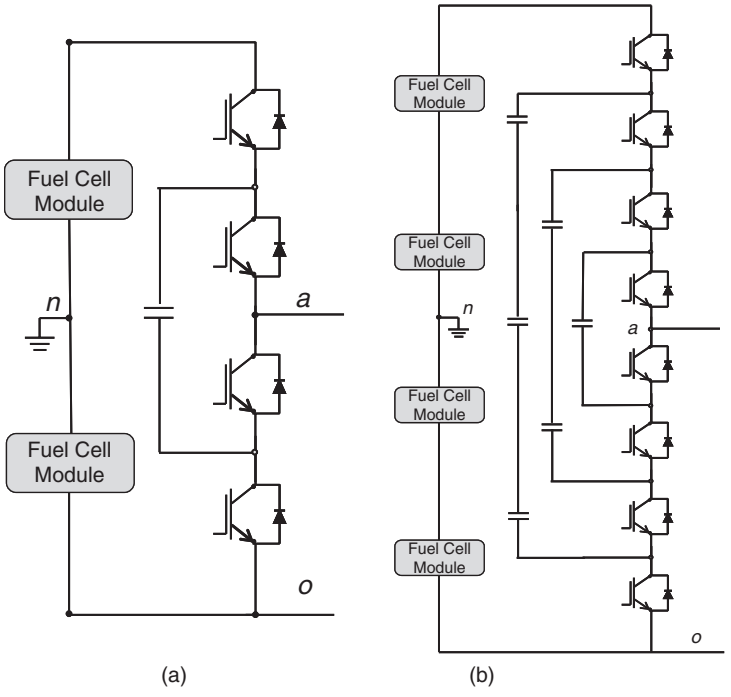


**FIGURE 28.19** Schematics of one phase leg fuel-cell PCS for high power applications using capacitor-clamped multilevel inverter: (a) three-level and (b) five-level inverter. Copyright © IEEE, 2002, Rodriguez etc. [27].

Figure 28.19 show diagrams of one phase leg multilevel capacitor-clamped inverter. The operational principle is similar to diode-clamped type multilevel except the clamping of device voltages is achieved by the flying capacitors [27]. Similar to diode-clamping, capacitor clamping requires a large number of bulk capacitors to clamp the voltage. For a $m$-level inverter, a total of $(m-1) \times (m-2)/2$ clamping capacitors are needed per phase leg.

Figure 28.20 shows a 24 MVA NPC inverter using integrated gate commutated thyristor (IGCT) series connection for medium-voltage applications [28]. Topology used here is a diode clamped three-level inverter with series connection of semiconductors. The overall input dc bus voltage $V_{dc}$ is 14.4 kV. To sustain this voltage, each switch is composed of three 4.5 kV IGCTs and each diode is made up of three 4.5 kV diodes. The RC snubbers are also used for the purpose of voltage balancing.

As compared to the other configurations, the series connection of fuel-cell modules followed by an inverter has less complexity and less number of semiconductor devices.

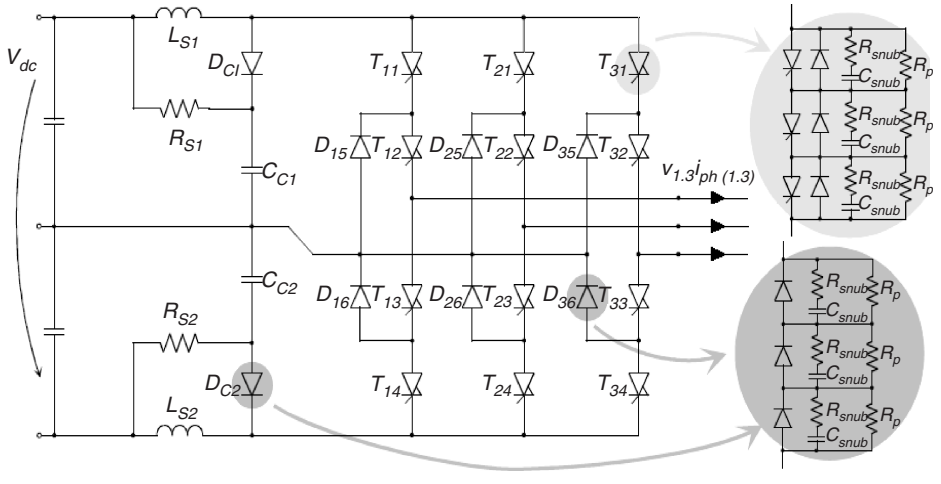


**FIGURE 28.20** A 24 MVA inverter using IGCT series connection for medium-voltage applications. Copyright © IEEE, 2001 Nagel etc. [28].

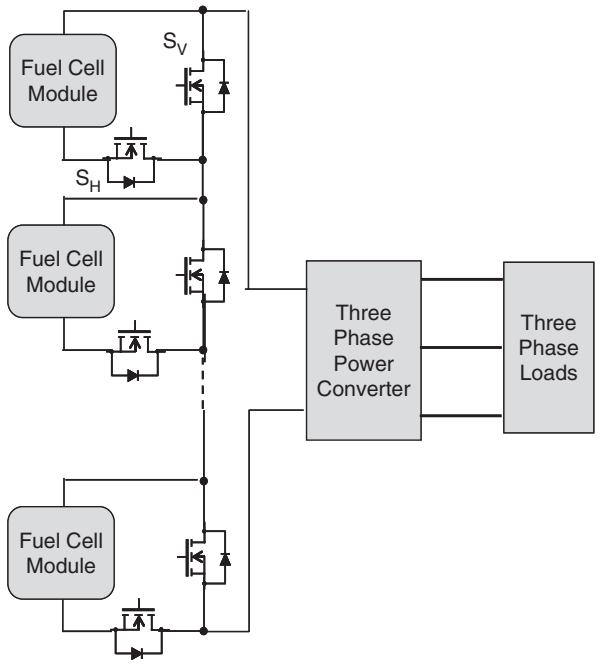


**FIGURE 28.21** Level reduction configuration of multiple fuel-cell modules to generate dc bus followed by a three-phase inverter [29, 30].

But the system has potential reliability problem since failure of one fuel cell can potentially make the whole system inoperable. So far, the power conditioning systems aforementioned have to sustain the variation of fuel-cell stack voltage caused by the change of loads. Since power semiconductor devices have to be selected for the highest input voltage, this degrades the device utilization and increases the cost by using more expensive higher voltage devices.

The problem can be alleviated by cascading the fuel-cell modules and dc/dc converters [29, 30]. As shown in Fig. 28.21, each fuel-cell module has an associated vertical ($S_V$) and a horizontal ($S_H$) switches. They are complementarily controlled. When $S_H$ is on and $S_V$ is off, the fuel-cell module supplies power. If $S_V$ is on and $S_H$ is off, the fuel-cell module is inhibited. With this configuration, the need for degrading power semiconductors in fuel-cell systems is reduced. By inhibiting some of the fuel cells and using the inhibited fuel cells in other applications, like charging batteries, the system efficiency and the fuel-cell utilization increases. It also has the advantages of increasing reliability. This means that if a fuel cell fails, the system will continue to operate. A three-phase inverter is still required for the voltage inversion. This inverter will require a variable modulation index to compensate for the varying dc bus voltage but this variation will not be as extreme as the one in Fig. 28.16.

A different converter configuration is introduced in [31], which is based on the series connection of single-phase inverters with separate dc sources (Fig. 28.22). Figure 28.22a shows a phase leg of a seven-level inverter with three cells in each phase. The output is formed by the combination of the ac voltages generated by each single-phase full-bridge inverter cell, which outputs three voltage levels: $+V_{dc}$, $-V_{dc}$, and 0 (Fig. 28.22b). Cascade multilevel converter can have several types of variation.

Figure 28.23 shows another way to achieve a voltage source multilevel inverter by voltage addition with transformers, which has been realized for high power applications [32, 33]. The step voltage waveforms are obtained by adding the each output of the inverter at the transformer secondary side. In this configuration, only one fuel-cell module is required. The isolation and voltage boost can be achieved by transformer. However, the transformer in this configuration requires special design and may saturate if the primary-side current has a dc component.

Figure 28.24a shows a mixed-level hybrid multilevel cell, obtained by replacing the full bridge of the cascade multilevel cell in Fig. 28.24 by diode-clamped or capacitor-clamped multilevel inverter. The number of the fuel cells is reduced by half. The dc voltage of fuel-cell modules in this configuration can be different which produces asymmetric hybrid multilevel cells. It is also possible to modulate different cells of cascade multilevel converter with different frequencies and implement it using different types of power devices, as shown in Fig. 28.24b.

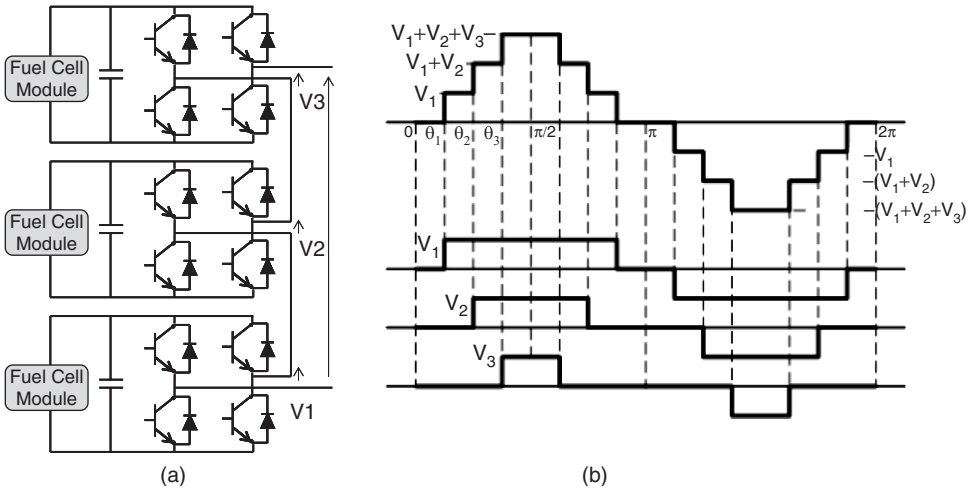


**FIGURE 28.22** Schematics of one phase leg fuel-cell PCS for high power applications using cascaded multilevel inverter: (a) diagram of seven-level cascaded multilevel inverter and (b) its corresponding waveforms. Copyright © IEEE, 2003, Ozpineci etc. [26].

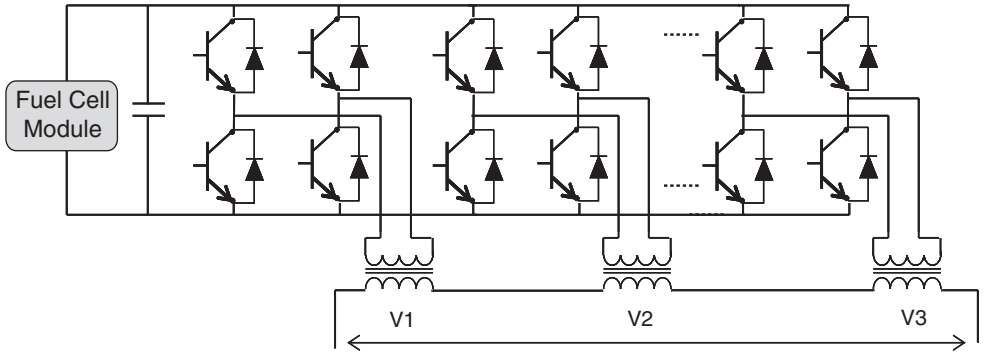


**FIGURE 28.23** Diagram of one phase leg of a voltage addition with transformer [32].

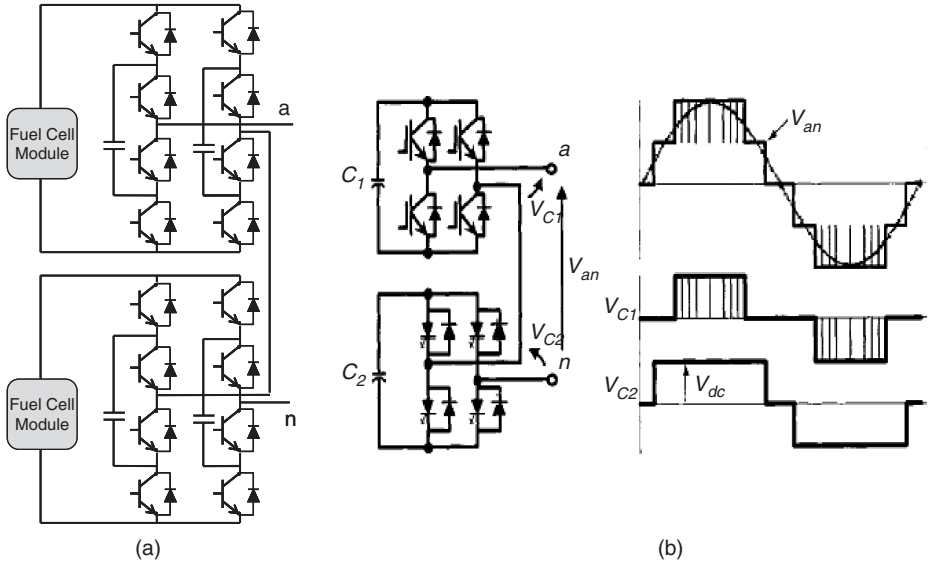


**FIGURE 28.24** Two variations of cascade multilevel converter: (a) a phase leg of asymmetric hybrid multilevel topology and (b) a phase leg of asymmetric cascaded multilevel topology. Copyright © IEEE, 2002, Rodriguez etc. [27].

## Acknowledgments

The work described in this paper is supported in parts by the California Energy Commission (CEC) under Award No. 53422A/03-02 and by the Department of Energy (DOE) under Award No. DE-FC2602NT41574. However, any opinions, findings, conclusions, or recommendations expressed herein are those of the authors and do not necessarily reflect the views of the CEC or DOE.

## References

1. http://www.pbworld.com/library/technical_papers/pdf/61_DieselEngine.pdf
2. http://www.eere.energy.gov/de/pdfs/ams_program_plan.pdf
3. http://www.eia.doe.gov/
4. G.K. Andersen, C. Klumpner, S.B. Kjaer, and F. Blaabjerg, "A new green power inverter for fuel cells", *IEEE Power Electronics Specialists Conference*, 2002, pp. 727–733.
5. R. Gopinath, S.S. Kim, and P. Enjeti, "Development of a low cost fuel cell inverter with DSP control", *IEEE Power Electronics Specialists Conference*, 2002, pp. 1256–1262.
6. G.W. Pradeep, H. Mohammad, and P. Famouri, "High efficiency low cost inverter system for fuel cell application", *Fuel Cell Seminar*, 2003. (Also available at http://www.energychallenge.org/FuelCellSeminar.pdf.)
7. J. Mazumdar, I. Batarseh, and N. Kutkut, "High frequency low cost dc-ac inverter design with fuel cell source for home applications", *IEEE Industry Applications Conference*, 2002, pp. 789–794.
8. A.M. Tuckey and J.N. Krase, "A low-cost inverter for domestic fuel cell applications", *IEEE Power Electronics Specialists Conference*, 2002, pp. 339–346.
9. P.T. Krein and R. Balog, "Low cost inverter suitable for medium-power fuel cell sources", *IEEE Power Electronics Specialists Conference*, 2002, pp. 321–326.
10. H. Ertl, J.W. Kolar, and F.C. Zach, "A novel multicell dc-ac converter for applications in renewable energy systems", *IEEE Transactions on Industrial Electronics*, 2002, pp. 1048–1057.
11. J. Wang and F.Z. Peng, "A new low cost inverter system for 5 kW fuel cell", *Fuel Cell Seminar,* 2003. (Also available at http://www.energychallenge.org/FuelCellSeminar.pdf.)
12. T.P. Bohn and R.D. Lorenz, "A low-cost inverter for domestic fuel cell applications", *Fuel Cell Seminar*, 2003. (Also available at http://www.energychallenge.org/FuelCellSeminar.pdf.)
13. T. Kawabata, H. Komji, and K. Sashida, "High frequency link dc/ac converter with PWM cycloconverter", *IEEE Industrial Application Society Conference,* 1990, pp. 1119–1124.
14. S. Deng and H. Mao, "A new control scheme for high-frequency link inverter design", *IEEE Applied Power Electronics Conference and Exposition*, 2003, pp. 512–517.
15. S. Ĉuk and R.W. Erickson, "A conceptually new high-frequency switched-mode amplifier technique eliminates current ripple", *Proceedings of Fifth National Solid-State Power Conversion Conference*, May 1978, pp. G3.1–G3.22.
16. S.K. Mazumder, R.K. Burra, and K. Acharya, *A novel efficient and reliable dc-ac converter for fuel cell power conditioning*, USPTO Patent Application# 20050141248, 2005.
17. S.K. Mazumder and R.K. Burra, "Fuel cell power conditioner for stationary power system: Towards optimal design from reliability, efficiency, and cost standpoint", Keynote Lecture, *ASME Proceedings on Third International Conference on Fuel Cell Science, Engineering and Technology*, 2005, FUELCELL2005-74178.
18. R.K. Burra, *A high performance power conditioner for solid-oxide fuel cell based stationary power generation*, Doctoral Dissertation, University of Illinois at Chicago, Chicago, Illinois, 2005.
19. S.K. Mazumder *et al.*, *Topic B: Design and development of a 1 kW fuel cell grid connected inverter*, Final Report, IEEE Future Energy Challenge Competition, 2005.
20. http:// www.eren.doe.gov/distributedpower
21. G.W. Pradeep, H. Mohammad, and P. Famouri, *et al.*, "High efficiency low cost inverter system for fuel cell application", *Fuel Cell Seminar*, 2003.
22. P.T. Krein and R. Balog, "Low cost inverter suitable for medium-power fuel cell sources", *IEEE Power Electronics Specialists Conference*, 2002, pp. 321–326.
23. A.M. Tuckey and J.N. Krase, "A low-cost inverter for domestic fuel cell applications", *IEEE Power Electronics Specialists Conference*, 2002, pp. 339–346.
24. R.D. Middlebrook and S. Ĉuk, *Advances in switched-mode power conversion*, vols. I, II, and III, TESLACO, 1983.
25. S.K. Mazumder *et al.*, "A low-cost single-stage isolated differential Cuk inverter for fuel cell application", submitted for review, *IEEE Power Electronics Specialists Conference*, 2005.
26. B. Ozpineci, Z. Du, L.M. Tolbert, D.J. Adams, and D. Collins, "Integrating multiple solid oxide fuel cell modules", *IEEE Industrial Electronics Conference*, 2003, pp. 1568–1573.
27. J. Rodriguez, J-S. Lai, and F.Z. Peng, "Multilevel inverters: A survey of topologies, controls, and applications", *IEEE Transactions on Industrial Electronics*, vol. 49, no. 4, 2002, pp. 724–738.
28. A. Nagel, S. Bernet, P.K. Steimer, and O. Apeldoorn, "A 24 MVA inverter using IGCT series connection for medium voltage applications", *IEEE Thirty-Sixth IAS Annual Meeting Conference Record*, 2001.
29. B. Ozpineci, L.M. Tolbert, and D. Zhong, "Optimum fuel cell utilization with multilevel inverters", *IEEE Power Electronics Specialists Conference*, 2004, pp. 4798–4802.
30. B. Ozpineci, L.M. Tolbert, G-J. Su, and Z. Du, "Optimum fuel cell utilization with multilevel dc-dc converters", *IEEE Applied Power Electronics Conference*, 2004, pp. 1572–1576.
31. P.W. Hammond, "A new approach to enhance power quality for medium voltage ac drives", *IEEE Transactions on Industry Applications*, vol. 33, no. 1, 1997, pp. 202–208.
32. S. Mariethoz and A. Rufer, "Design and control of asymmetrical multi-level inverters", *IEEE Industrial Electronics Conference*, 2002 pp. 840–845.
33. N.P. Schibli, T. Nguyen, and A.C. Rufer, "A three-phase multilevel converter for high-power induction motors", *IEEE Transactions on Power Electronics*, vol. 13, no. 5, 1998, pp. 978–986.